Journal of Computational Electronics (2023) 22:1715–1724
https://doi.org/10.1007/s10825-023-02106-9

Optimization of CdS-free non-toxic electron transport layer for Sb_2S_3-based solar cell with notable enhanced performance

Sameen Maqsood[1,2] · Zohaib Ali[1] · Khuram Ali[1] · Rimsha Bashir Awan[3] · Yusra Arooj[2] · Ayesha Younus[2]

Received: 5 October 2022 / Accepted: 28 September 2023 / Published online: 20 October 2023

Abstract

In this investigation, we develop CdS-free non-toxic thin-film solar cell structure with antimony sulfide (Sb_2S_3) as an absorber material. Sb_2S_3 has found to be a promising candidate for production of renewable energy. Solar cells based on Sb_2S_3 have been attracted worldwide attraction due to their outstanding efficiency and low cost. To serve as an optimistic buffer layer, 3C-SiC (cubic silicon carbide) is used thanks to its suitable bandgap to replace toxic cadmium sulfide (CdS). SCAPS-1D (one-dimensional solar cell capacitance simulator) software has been employed to numerically investigate the performance of Sb_2S_3-based n-ZnO/n-3C-SiC/p-Sb_2S_3 heterostructure solar cells. The influence of absorber/buffer layer thickness, acceptor/donor densities, and defect density on device working have been investigated. Consequently, the role of defects in p-Sb_2S_3 along with the significance of n-3C-SiC/p-Sb_2S_3 interface defects has been studied to provide recommendations for achieving high efficiency. The proposed structure provides the enhanced efficiency of 17% under 1.5 G illumination spectrum. The parameters regarding solar cell performance such as V_{oc}, J_{sc}, FF, QE and η have been studied graphically. This novel structure may have considerable influence on progress of improved photovoltaic devices in future.

Keywords 3C-SiC · Sb_2S_3 · Buffer layer · Efficiency · Absorber layer · SCAPS-1D

1 Introduction

Photovoltaic devices have attracted a huge attention worldwide for successive energy harvesting due to several benefits including everlasting power at least working cost, long lifetime, very less pollution, lower maintenance and easy to use [5]. Thin-film solar cells are the most prominent candidate in photovoltaics due to their low-cost production, lower maintenance, high efficiency, user friendly and most importantly low pollution [6–12]. In the production of commercial TFSCs, many materials are used as absorbing layers like silicon [13–17], Cu(In,Ga)Se_2 [18, 19], $Cu_2ZnSn(S,Se)_4$ [20–22] CdTe [23–26]. However, the problem remains in the manufacturing of highly efficient TFSCs using these absorbing layers due to high cost, low abundancy, and high toxicity. Several investigations have been made to overcome these challenges by finding new absorbing materials in the application of TFSCs that have properties such as highly abundance, cost-efficiency, environment-friendly, and high stability [27–31]. Selenium (Se) has recently gained interest of global research groups due to its wide bandgap (1.8 eV) and intrinsic environmental stability [32]. Though, the melt processing limits the use of Se to some extents due to its deprived wettability which melt Se on top of some materials such as TiO_2. Antimony Sulfide (Sb_2S_3) is a newly found optimal absorbing material in the application of TFSCs due to good career mobility [33–37], high abundancy, ideal absorption coefficient (10^5 cm^{-1}), propitious range of band gap (1–1.2eV), cost-efficient and less toxic [33, 35, 38–41]. In several theoretical [42–47] and experimental [33, 37, 38, 48–55], the auspicious performance of p-Sb_2S_3 as absorbing material has been reported. The performance efficiency of 7.23% was achieved by employing liquid medium annealing

✉ Zohaib Ali
zohaibali999@yahoo.com

✉ Khuram Ali
khuram_uaf@yahoo.com

1 Nano-Optoelectronics Research Laboratory, Department of Physics, University of Agriculture, Faisalabad 38040, Pakistan

2 Department of Physics, Government College Women University Faisalabad, Faisalabad, Pakistan

3 Department of Sciences and Humanities, National University of Computer, and Emerging Sciences (FAST) Chiniot Faisalabad Campus, Chiniot, Pakistan

[1]. With device scheme of ITO/TiO_2/Zn(O,S)/Sb_2S_3/Carbon/Ag, 3.7% efficiency has been achieved by using in situ hydrothermal deposition [2]. 8% efficiency was obtained by using unique chemical bath deposition technique which improves the deposition rate, crystallinity and film morphology as well [3]. Vertically oriented thin-films obtained on various buffer layers and 4.37% efficiency have been achieved with structure (ITO)/CdS/Sb_2S_3/Au [4]. The 2.26% maximum efficiency was achieved by using TiO_2 as buffer layer in FTO/TiO_2/Sb_2Se_3/Au-based solar cells [38]. On experimental basis, heterojunction solar cell with Sb_2Se_3 3.21% efficiency was achieved [48]. The PCE (%) of 2.1% was obtained by using glass/-FTO/TiO_2/Sb_2Se_3/CuSCN/Au-based solar cells, where HTL was CuSCN [50]. The maximum conversion efficiency of 5.6% was achieved by applying thermal evaporation method in glass/-FTO/CdS/Sb_2Se_3/Au-based solar cells [33]. The PCE (%) of 7.6% was obtained with ITO/CdS/Sb_2Se_3/Au solar cells that were designed by vapor transport deposition technique [54]. Germanium mono-selenide (GeSe), another promising material, has been used to obtain the efficiency of 3.1% with device configuration of Glass/ITO/CdS/GeSe/Au. A substrate special arrangement adopted that allows CdS pre-deposition on top of polycrystalline GeSe layer at room temperature and avoid the diffusion of Cd [56]. A suitable buffer layer or window can be chosen on the basis of high optical transmittance and electric conductivity which enhance the efficiency but also protect it from damages [57]. In this respect, cubic silicon carbide (3C-SiC) is one of the most prominent candidates as a buffer material or window in TFSCs application due to its bandgap of 2.36 V [58]. The great electronic properties of 3C-SiC have been reported in comparison with other buffer materials like SiC. The distinctive property of 3C-SiC is that it has 10^{16} cm^{-3} of intrinsic concentration at 300 K and can be n- doped with Ga, Al, and B dopants. [59–61]. High efficiency of 25.51% has been reported in a recent simulation study in CIGS TFSCs which was modeled with a buffer layer or window with 3C-SiC [62]. Therefore, the performance of heterojunction solar cell-based 3C-SiC/Sb_2S_3 is investigated by the theoretical approach.

In this study, the main objective is to study the feasibility of 3C-SiC/Sb2S3 heterojunction photovoltaic cell. The simulation tool was used for the vast and complex optimized design of the Sb_2S_3-based photovoltaic cell. The Scaps-1D has been utilized to enhance chronologically the configuration of the photovoltaic cell by exploring defect density, outcome of doping concentration, and width of buffer layer or window 3C-SiC and absorber Sb_2S_3. To prevent any degradation in analyzing the solar cell operation, changes in operating temperature have been made in the range.

This paper consists of methodology, results, and conclusion. In the methodology section, we introduced the parameter values, model, and formulation of heterostructure solar cells by using simulation in SCAPS-1D. In the result section, we plotted the parameters of proposed structures such as Fill factor (FF), Short-circuit current density (J_{sc}), open-circuit voltage (V_{oc}), and efficiency (η). The last section is based on a conclusion and summary.

2 Methodology

One-dimensional solar cell capacitance simulator (SCAPS-1D) [63] has been utilized to develop and examine the Sb_2S_3-based photovoltaic device. It solves continuity and Poisson equations for electrostatic potential and free carriers (holes/electrons) for heterojunction devices. These equations are given below,

$$\frac{\partial}{\partial x}\left(\varepsilon_0\varepsilon\frac{\partial \Psi}{\partial x}\right) = -q\left(p - n + N_D^+ - N_A^- + \frac{\rho_{def}}{q}\right) \tag{1}$$

$$-\frac{\partial J_n}{\partial x} - U_n + G = \frac{\partial n}{\partial t} \tag{2}$$

$$-\frac{\partial p}{\partial x} - U_p + G = \frac{\partial p}{\partial t} \tag{3}$$

Here, Ψ is the electric potential, ε is permittivity, charge represented by q, N_a and N_d are the acceptor and donor densities, p and n are holes and electron densities, G is the generation rate, and J_p and J_n are the current densities for holes and electrons, respectively. The performance of device limitations such as recombination profile, J–V (current density–voltage) characteristics, energy band diagram and quantum efficiency can be defined by solutions of equations. The numerical simulation is carried out under 100 mW cm^{-2} illumination, with 300 K temperature and air mass AM 1.5 G to analyze the working of device. In the present work, 3C-SiC buffer layer has been introduced as the replacement of CdS layer. The comparison has been made to analyze the design of optimized heterostructure solar cell. The representation of Sb_2S_3-based heterojunctions of Al/ZnO/3C-SiC/Sb_2S_3/Mo is shown in Fig. 1b.

The structure contains window layer of ZnO with energy bandgap of 3.30 eV, the buffer layer of n-type 3C-SiC with bandgap of 2.62 eV [58] and p-Sb_2S_3 as absorber with bandgap of 1.62 eV [64]. The transfer of hole and electron beyond the heterostructure can be significantly determined by band structure analysis. SCAPS-1D offers the energy band configuration for the suggested heterostructure of device. The related parameters to material characteristics employed in this work were extracted from experimental and theoretical studies reported earlier [58, 64, 65] and also described in Table 1. The factors such as layer thickness, defect density and doping concentration of buffer and absorber layer

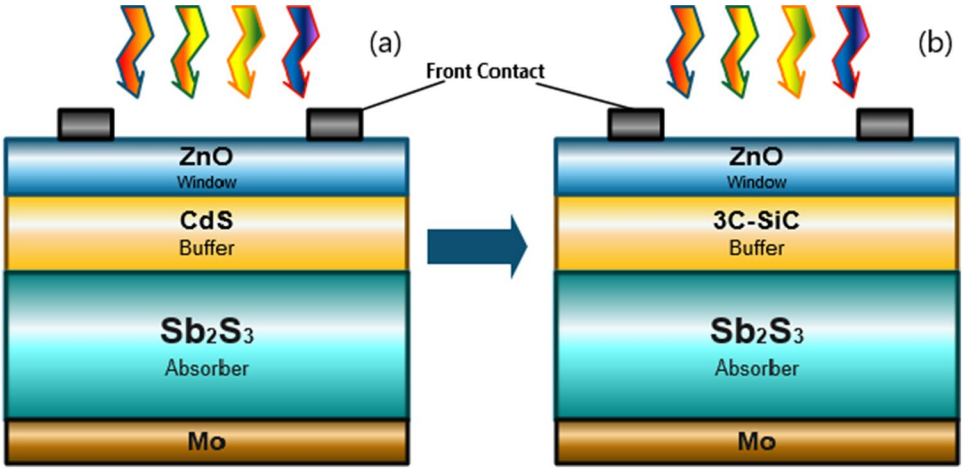

Fig. 1 Schematic diagram of Sb_2S_3-based solar cell with CdS and 3C-SiC buffer layer

Table 1 Parameters affecting the device performance and simulation values

Factors (unit)	ZnO	3C-SiC	Sb_2S_3
Thickness w(μm)	0.05	0.05	2.0
E_g(eV)	3.30	2.36	1.62
χ(eV)	4.6	3.38	3.7
ε_r	8.9	9.72	7.08
N_c (cm^{-3})	2.2×10^{18}	1.5×10^{19}	2×10^{19}
N_v (cm^{-3})	1.8×10^{19}	1.2×10^{19}	1×10^{19}
Thermal velocity (electron cm/s)	1×10^{7}	2×10^{7}	1×10^{7}
Thermal velocity (hole cm/s)	1×10^{7}	1.5×10^{7}	1×10^{7}
μ_n (cm^2/Vs)	100	400	9.8
μ_p(cm^2/Vs)	25	50	10
N_D (cm^{-3})	10^{19}	10^{16}	0
N_A (cm^{-3})	0	0	5.752×10^{15}

and absorber-buffer interface have been changed involving the device structure. The variables defining performance of device such as J–V characteristics, band profile and quantum efficiency (QE) are obtained from the findings and improved. The influence of Sb_2S_3 absorber and 3C-SiC layer thickness was analyzed. Furthermore, the influence of operating temperature on performance of device has been also examined.

Energy band diagram for Sb_2S_3-based solar cell along with 3C-SiC and CdS buffer layers is demonstrated in Fig. 2b and a, respectively. In Fig. 2a, one can notice a "spike" at Sb_2S_3/CdS junction which is a positive conduction band offset (ΔEc). The lower portion of conduction band gets closer to the Fn (quasi-fermi level) for electrons due to the spike as shown in Fig. 2a. It needs a larger bending in valence band which leads in induction of wider barrier for the holes reaching the interface. In addition, at CdS/ZnO interface the negative conduction band offset increases the chance of recombination which directly affects the device performance.

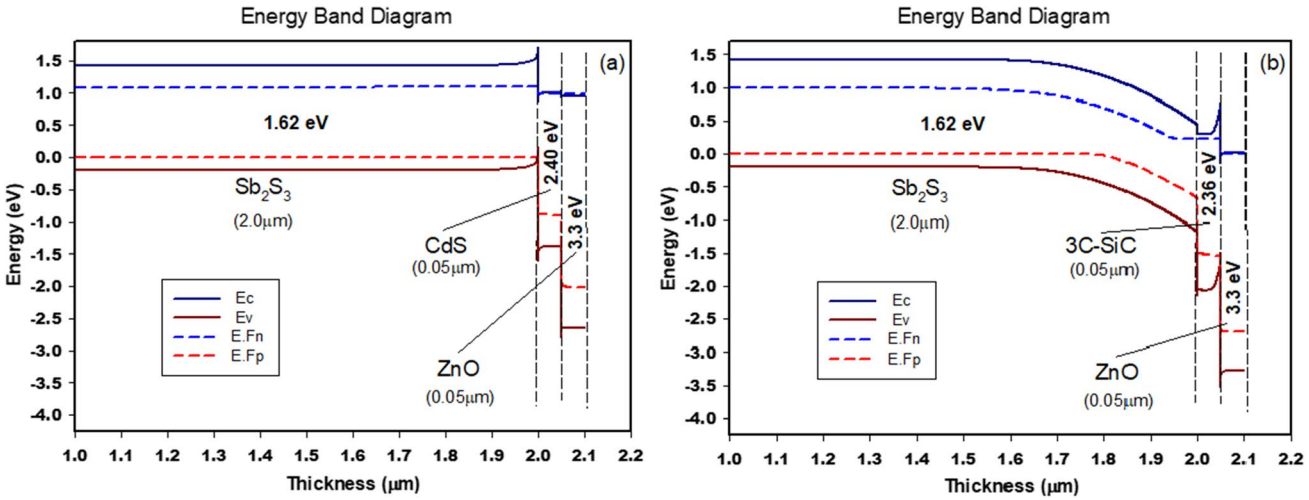

Fig. 2 Bandgap schema of Sb_2S_3-based heterojunction solar cell with buffer layer (3C-SiC)

3 Results

The key motive of this study is to examine the effect of several aspects of absorber and buffer width on working of Sb_2S_3 based photovoltaic cells. Application of the improved data will assist us to resolve a set of constraints for real time model of solar cell with an optimum conversion efficiency. The simulation and design were assembled for optimization of defect density, thickness, and doping concentrations of *n*-3C-SiC buffer and *p*-Sb_2S_3 absorber layer. The conduction band offset at the 3C-SiC/Sb_2S_3 junction is due to difference between the electron affinities of 3C-SiC and Sb_2S_3 materials. In this way, photoelectrons move toward the 3C-SiC layer from *p*-Sb2S3 before recombination with the holes.

A comparison of simulation results has been made for CdS and 3C-SiC buffered solar cell in Fig. 3. It represents the analysis of J–V (current density and voltage) characteristics and Spectral response for proposed structure. The thicknesses of Sb_2S_3, 3C-SiC and ZnO layers are 2 µm, 0.05 µm and 0.05 µm, respectively. One can notice that the voltage and current density for proposed heterostructure with 3C-SiC buffer layer is good than the device with CdS layer. The V_{oc} with CdS layer is determined to be 1.08 V with J_{sc} of 22.64 mA/cm^2, FF of 58% and efficiency of 14%, whereas the enhanced V_{oc} of 1.4 V, J_{sc} of 23.52 mA/cm^2, FF 47% and efficiency of 17.18% has been obtained for the PV cell structure with 3C-SiC layer. The spectral response (quantum efficiency) of both device structures is illustrated in Fig. 2b. The wavelength is changing from 300 to 800 nm to calculate spectral response. It is clear from results that change of buffer layer does not affect the spectral response of solar cell significantly. However, it can be improved by introducing a hole transport layer (HTL) or back surface field (BSF) layer at rear of device [66] which would be incorporated in future investigations. The spectral response attained at the range of short wavelength in this work, which is in good agreement with previous studies reported earlier [66–68]. By introducing 3C-SiC buffer layer, a significant improvement in the solar cell performance parameters has been realized. Therefore, all the simulations by changing parameters are carried out for ZnO/3C-SiC/Sb_2S_3/Mo heterostructure.

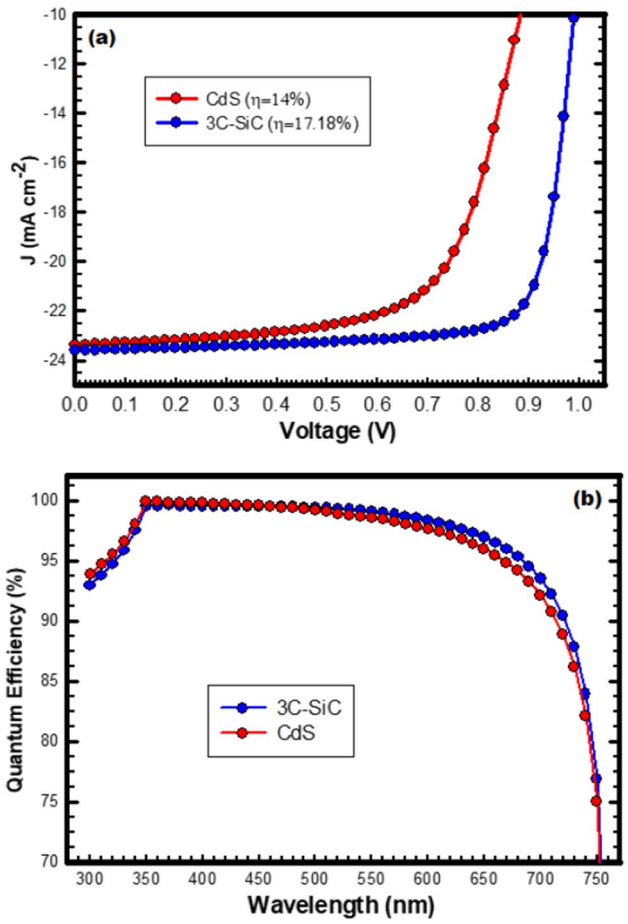

Fig. 3 Represents the **a** J–V analysis, **b** Quantum efficiency of CdS and 3C-SiC buffered solar cell

3.1 Optimization of buffer layer (3C-SiC) thickness

The thickness of 3C-SiC layer changes to analyze the functioning of Sb_2S_3 solar cell. The width of buffer layer varies from 10 to 100 nm with 10 nm each step size. The buffer layer should be narrower to decrease the impact of series resistance [69]. The influence of 3C-SiC layer thickness on η, FF, V_{oc} and J_{sc} has been analyzed, as displayed in Fig. 4a, b. The highest efficiency of 17% has been achieved for layer thickness of 0.05 µm, while J_{sc} firstly show a minor increase and then, very slight decrease from 23.5 to 23.4 mA/cm^{-2}. The V_{oc} increases with a large step from 1.1 to 1.5 V at start; with further rise in buffer layer width, it shows very minor change in the entire range. The nearly constant J_{sc} value can be explained as the thickness of 3C-SiC layer rises which give growth in absorption of photons at more distance of Sb_2S_3/3C–SiC junction with shorter wavelength. It reduces intensity of photons which are strong enough to penetrate to Sb_2S_3 layer [70–72]. Figure 4b illustrates that FF noticeably decreases from 55 to 47% as thickness of increases from 10 to 20 nm of buffer layer. Further increment in thickness of buffer layer does not affect the FF, so the optimized value for layer thickness is considered 0.05 µm. FF and J_{sc} have an inverse relationship; both parameters trivially vary in opposite trends as thickness increases. The rise in the thickness of 3C-SiC layer has a negative impact on efficiency, indicating the increase in absorption of photons in the buffer layer. As a result, fewer number of photons approached to the Sb_2S_3 layer which led to decrease the production of electron–hole pair. The overall performance of the Sb_2S_3-based solar cell improves with the addition of a 3C-SiC layer as a buffer

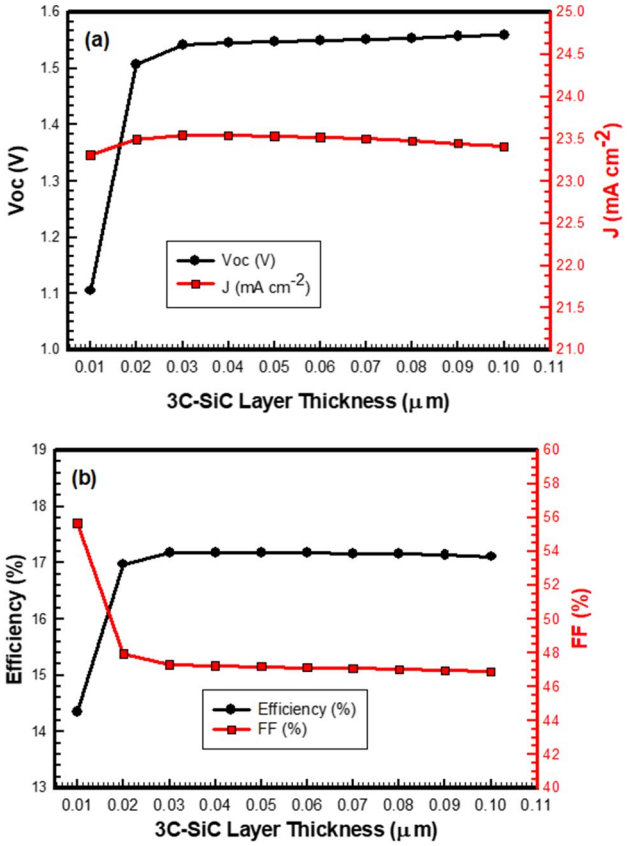

Fig. 4 Optimization of buffer layer (3C-SiO) thickness in terms of **a** V_{oc} and J_{sc} **b** Efficiency and FF

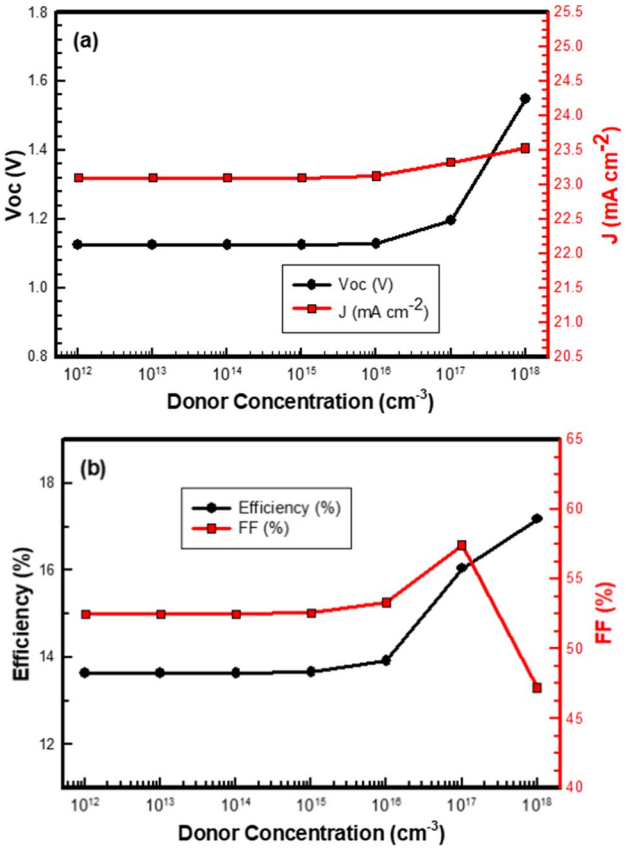

Fig. 5 Optimization of donor density (N_D) of buffer layer (3C-SiO) in terms of **a** V_{oc} and J_{sc} **b** Efficiency and FF

layer instead of CdS, but all other parameters showed insignificant change with change in the thickness of buffer layer.

3.2 Optimization of doping concentration of buffer layer (3C-SiC)

To investigate the influence of donor doping concentration (N_D) in 3C-SiC layer on solar cell performance, N_D varies from 10^{12} to 10^{18} cm^{-3} as demonstrated in Fig. 5. The value of V_{oc} is almost constant in the range of 10^{12}–10^{16} cm^{-3}; then, it increases with the further increase in donor concentration. As a result, increase in non-recombination losses, causing the saturation J_{sc} to rise. Therefore, the value of V_{oc} significantly increases as the donor concentration varies [73]. Figure 5a also shows how J_{sc} responds to variations in the doping concentration of the 3C-SiC layer. With the increase in donor concentration, the J_{sc} exhibits the similar trend as of V_{oc}, it remains unchanged for the range of N_D from 10^{12} to 10^{16} cm^{-3} and then, slightly increases due to reduction in carrier diffusion length [74]. Figure 5b shows the variation in FF as donor concentration changes. FF exhibits notable increment from 53.3 to 57.4% from 10^{16} to 10^{17} cm^{-3} and rapidly decreases for higher values of donor concentration till 10^{18} cm^{-3}. This behavior is in view of the fact that large carrier concentration increases recombination losses at junction [73]. Figure 5b illustrated the efficiency against the doping concentrations of buffer layer. The efficiency increases monotonically as the doping concentration increases from till 10^{16} to 10^{18} cm^{-3}. Hence, the optimal value of doping concentration for buffer layer is 1.0×10^{18} cm^{-3}.

3.3 Optimization of thickness of absorber layer (p-Sb_2S_3)

The thickness of absorber layer (Sb_2S_3) plays a significant aspect to achieve the maximum PCE (%) of 3C-SiC/Sb_2S_3 heterojunction solar cell. The influence of changing absorber layer thickness on J_{sc}, V_{oc}, η and FF is analyzed and demonstrated in Fig. 6. The J_{sc} and V_{oc} increase as the absorber layer thickness increases from 1.0 to 2.0 μm. The V_{oc} and J_{sc} show a rapid increment till 2.0 μm and then, slightly increases for higher values, which shows a non-significant behavior as demonstrated in Fig. 6a. The efficiency shows almost the same behavior with the increase in absorber layer thickness from 1.0 to 2.0 μm demonstrated in Fig. 6b. One can notice

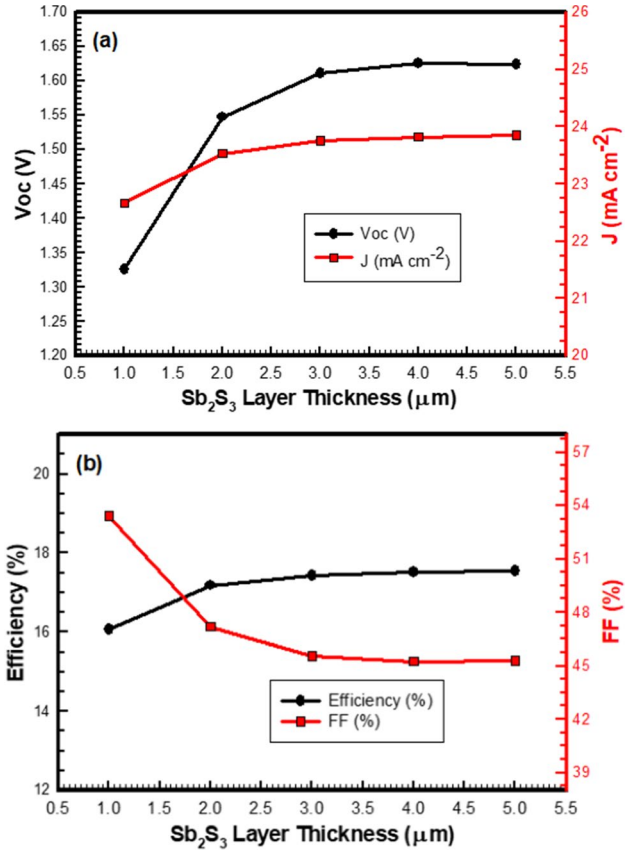

Fig. 6 Optimization of absorber layer (Sb_2S_3) thickness in terms of **a** V_{oc} and J_{sc} **b** Efficiency and FF

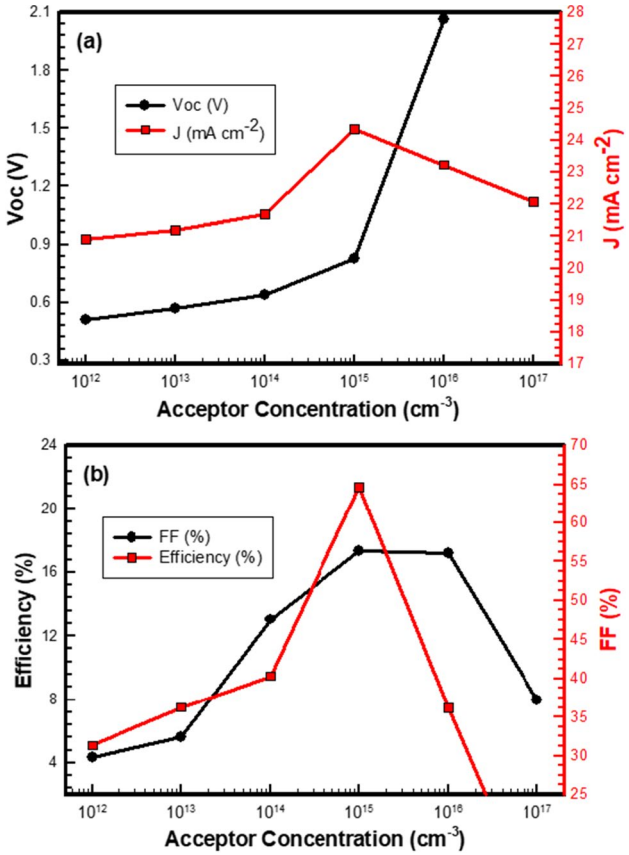

Fig. 7 Optimization of acceptor density (N_A) for absorber layer (Sb_2S_3) in terms of **a** V_{oc} and J_{sc} **b** Efficiency and FF

the decreasing trend of FF from 53.61 to 47.43% for initial increase in layer thickness from 1.0 to 2.0 µm, and non-significant variation for further higher value of layer width. However, the efficiency rapidly rises from 16 to 17% with change in thickness from 1.0 to 2.0 µm of absorber layer. For further increase in p-Sb_2S_3 layer up to 2.0 µm does not affect the efficiency significantly. This enhancement in the device performance is due to more absorption of photon and hole-electron production in the p-Sb_2S_3 layer. When the thickness exceeds the optimal value of absorber layer, the path length moved by photo-generated carriers becomes very large, resulting in more recombination. The optimal value of thickness is 2.0 µm for absorber layer for efficient and low-cost heterojunction solar cell. The results show good agreement with earlier reported results [75–78]. The carrier generation becoming less effective than carrier recombination for thick absorber which is responsible for J_{sc} saturation [64].

3.4 Optimization of doping concentration of absorber layer (Sb_2S_3)

The impact of variation in acceptor doping concentration (N_A) of absorber layer (p-Sb_2S_3) on 3C-SiC/Sb_2S_3 heterostructure device is demonstrated in Fig. 7. Higher values more than 10^{15} and lower values less than 10^{14} distinctively affect the optoelectronic properties of absorber layer. Highest efficiency for absorber layer of about 17.3% is recorded when doping concentration is 10^{15} cm^{-3}. Efficiency increases linearly when N_A rises from 10^{13} cm^{-3} because there is an increase in carrier concentration generation as a result of an increase in doping concentration. [79]. The value of current density (J_{sc} = 24.38 mA/cm^2) at 10^{15} cm^{-3} and continuous drop to 22.12 mA/cm^2 at 10^{18} cm^{-3} has been observed. With an increase in acceptor density, holes become more prevalent in the absorber layer, generating the hole trap center within the absorber layer. This enhances photo-generated electron recombination due to the attraction between the hole and electron, as a result the current density decreases as acceptor concentration increases.

Rashed et al. [76] for Sb_2S_3 heterojunction solar cell and Wanda et al. [71] for CZTS-based solar cell previously reported a similar behavior with modification of N_A in absorber layer. FF and efficiency increase as the acceptor concentration in absorber layer increases as illustrated in Fig. 7a. FF shows a similar behavior of reduction as J_{sc} for N_A more than 10^{15} cm^{-3}. The linear increase in solar cell

efficiency is caused by the rising trends in V_{oc} along with the increase in acceptor concentration of absorber layer.

3.5 Optimization of temperature on ZnO/3C–SiC/Sb_2S_3 solar cell

The operating temperature is responsible for controlling photovoltaic cell performance. When the operating temperature is high, the carrier concentration rises that results in increasing the rate of internal carrier recombination. Therefore, it is typically observed that device performance decreases as temperature rises [80–82]. As indicated in the literature, the temperature has a significant impact on the stability of solar cell, with the intent that open-circuit voltage varies with temperature change [83]. In this study, the operating temperature has been adjusted between 300 and 400 K to examine device performance as illustrated in Fig. 8. The value of V_{oc} drops as the temperature increases due to rise in recombination as shown in Fig. 8a [81, 84]. With the increase in temperature, value of V_{oc} linearly decreases from 1.542 to 0.961 V and J_{sc} does not show a significant variation a minor increase from 23.5 to 23.7 mA/cm^2 has been noticed. High temperatures reduce the bandgap of material and generate significant band-to-band absorption coefficients across the spectrum [80, 81] increasing leakage current and resulting in performance degradation of device. The impact of variation of temperature on FF has been analyzed as illustrated in Fig. 8c. The increment in cell temperature has a unique influence on cell parameters like FF, V_{oc} and η. FF increases as the operating temperature rises due to improving collisions and carrier recombination [84]. Figure 8d depicts the degradation in η with an increment in temperature, which is primarily due to a decrease in bandgap [83]. The parameters like η, FF, V_{oc} and J_{sc} validate that the proposed ZnO/3C–SiC/Sb_2S_3 solar cell can work efficiently at 400 K high operating temperature.

3.6 Optimization of total defect density of absorber layer (Sb_2S_3)

The solar cell performance has significantly influenced by defect density (Nt). The current produced by incident photons is significantly produced due to p-Sb_2S_3 (absorber layer). Therefore, when defect density rises, carries recombination also rises, which has an impact on the device efficiency. To investigate the variation in device performance, we vary the defect density from 10^{12} to 10^{16} cm^{-3} (see Fig. 9). All parameters (J_{sc}, V_{oc}, and η) begin to decrease for defect density values greater than 10^{15} cm^{-3} as demonstrated in Fig. 9. However, one can notice that FF starts increasing particularly at 10^{14} cm^{-3}, which is due to increase in energy barrier height [85]. The device performance is particularly sensitive to defect density because it generates multiple recombination centers, which improves carrier recombination and consequently reduces carrier lifetime. These recombination centers reduce the production of e–h by preventing the carriers from accessing the junctions. Hence, the overall performance of purposed solar cell decreases. The results are consistent with previous literature [78, 86].

4 Conclusion

This study has generated a graphical depiction through numerical analysis. The 3C-SiC has been shown to be a non-toxic prospective material for buffer layer in Sb_2S_3-based heterojunction solar cells. The SCAPS-1D simulator has been used to simulate the ZnO/3C-SiC/Sb_2S_3-based solar

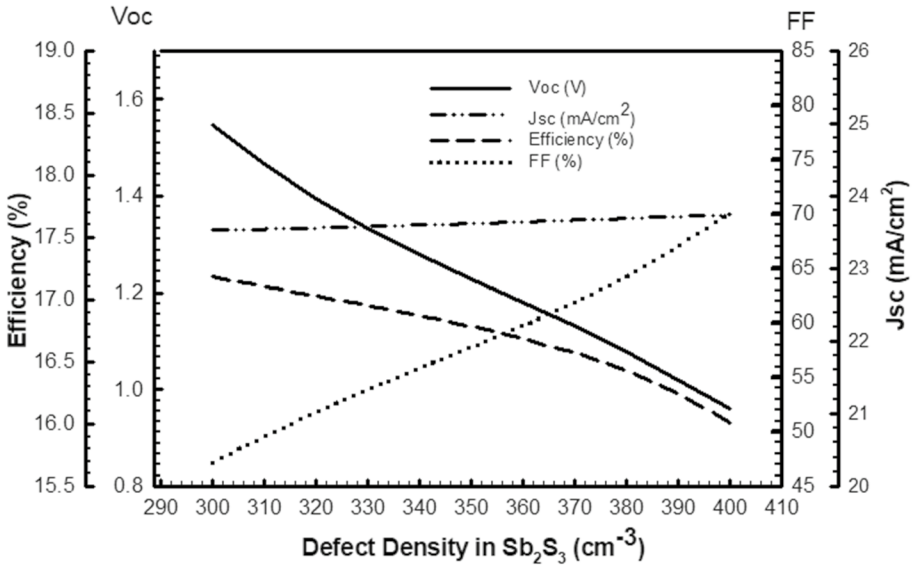

Fig. 8 Optimization of operating temperature in terms of **a** V_{oc}, **b** J_{sc} **c** FF, **d** Efficiency

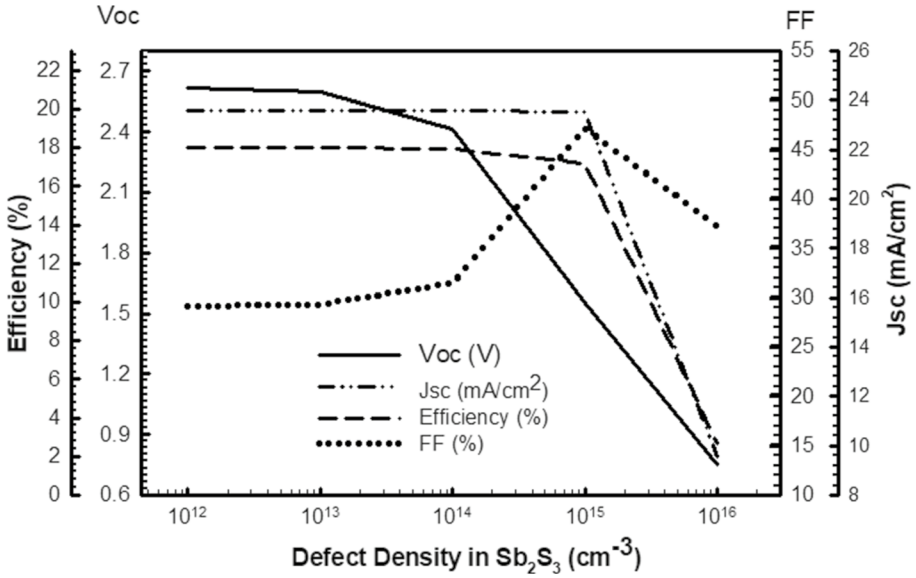

Fig. 9 Optimization of total defect density (N_t) of absorber layer (Sb_2Se_3)

cell. Device performance has been investigated by analyzing different parameters like thickness of layers, doping concentrations, operating temperature, and defect density. The impact of buffer layer (3C-SiC) and absorber layer (Sb_2S_3) thickness on FF, V_{oc} η, and J_{sc} of solar cell has been analyzed. To provide guidance for achieving optimum conversion efficiency, the defects come across in 3C-SiC and Sb_2S_3 layers as well as the role of 3C-SiC/Sb_2S_3 interface defects density have been thoroughly examined. The results demonstrate that the efficiency of solar cell with thin buffer layer (3C-SiC) has been improved. The thickness of 3C-SiC layer from 20 to 100 nm was varied to check its viability for optimum conversion efficiency. Maximum 17% conversion efficiency has been obtained with proposed solar cell which contain of ZnO/3C-SiC/Sb_2S_3 layers under 1.5 G illumination spectrum. The proposed structure could make a significant contribution in the field of photovoltaic devices in the future.

Acknowledgements This work was supported by the Higher Education Commission (HEC) of Pakistan [Grant No: 8615/Punjab/NRPU/R&D/HEC/2017] to Dr. Khuram Ali. The authors would like to acknowledge Dr. Marc Burgelman, University of Gent, Belgium, for providing the SCAPS simulator.

Data availability Enquiries about data availability should be directed to the authors.

Declarations

Conflict of interest The authors have not disclosed any conflict of interest.

References

1. Yao, L.-Q., et al.: A liquid medium annealing strategy for highly [041]/[141]-oriented planar antimony sulfide solar cells with 7.23% efficiency. Nano Energy **106**, 108064 (2023)
2. Lin, W., et al.: Zn (O, S) buffer layer for in situ hydrothermal Sb2S3 planar solar cells. ACS Appl. Mater. Interfaces **13**(38), 45726–45735 (2021)
3. Wang, S., et al.: A novel multi-sulfur source collaborative chemical bath deposition technology enables 8%-efficiency Sb2S3 planar solar cells. Adv. Mater. **34**(41), 2206242 (2022)
4. Zeng, Y., et al.: Quasi-vertically-orientated antimony sulfide inorganic thin-film solar cells achieved by vapor transport deposition. ACS Appl. Mater. Interfaces **12**(20), 22825–22834 (2020)
5. Espinosa, N., et al.: Outdoor fate and environmental impact of polymer solar cells through leaching and emission to rainwater and soil. Energy Environ. Sci. **9**(5), 1674–1680 (2016)
6. Chopra, K., Paulson, P., Dutta, V.: Thin-film solar cells: an overview. Prog. Photovoltaics Res. Appl. **12**(2–3), 69–92 (2004)
7. Aberle, A.G.: Thin-film solar cells. Thin Solid Films **517**(17), 4706–4710 (2009)
8. Chatzisideris, M.D., et al.: Ecodesign perspectives of thin-film photovoltaic technologies: a review of life cycle assessment studies. Sol. Energy Mater. Sol. Cells **156**, 2–10 (2016)
9. Lee, T.D., Ebong, A.U.: A review of thin film solar cell technologies and challenges. Renew. Sustain. Energy Rev. **70**, 1286–1297 (2017)
10. Medina-Montes, M., et al.: Development of sputtered CuSbS2 thin films grown by sequential deposition of binary sulfides. Semicond. Sci. Technol. **33**(5), 055004 (2018)
11. Sundaram, S., Shanks, K., Upadhyaya, H.: Thin film photovoltaics. In: A comprehensive guide to solar energy systems, pp. 361–370. Elsevier (2018)
12. Powalla, M., et al.: Thin-film solar cells exceeding 22% solar cell efficiency: an overview on CdTe-, Cu (In, Ga) Se2-, and perovskite-based materials. Appl. Phys. Rev. **5**(4), 041602 (2018)
13. Xu, M., et al.: Simple emitter patterning of silicon heterojunction interdigitated back-contact solar cells using damage-free laser ablation. Sol. Energy Mater. Sol. Cells **186**, 78–83 (2018)
14. Xu, M., et al.: Dry passivation process for silicon heterojunction solar cells using hydrogen plasma treatment followed by in situ a-Si: H deposition. IEEE J. Photovolt. **8**(6), 1539–1545 (2018)

15. Cho, J., et al.: Passivating electron-selective contacts for silicon solar cells based on an a-Si: H/TiOx stack and a low work function metal. Prog. Photovolt. Res. Appl. **26**(10), 835–845 (2018)
16. Xu, M., et al.: Silicon heterojunction interdigitated back-contact solar cells bonded to glass with efficiency> 21%. Sol. Energy Mater. Sol. Cells **165**, 82–87 (2017)
17. Abdo, I., et al.: Influence of periodic surface nanopatterning profiles on series resistance in thin-film crystalline silicon heterojunction solar cells. IEEE J. Photovolt. **5**(5), 1319–1324 (2015)
18. Bouich, A., et al.: Experimental, theoretical, and numerical simulation of the performance of CuInxGa (1–x) S2-based solar cells. Optik **183**, 137–147 (2019)
19. Kosyachenko, L.A., et al.: Optical and recombination losses in thin-film Cu (In, Ga) Se2 solar cells. Sol. Energy Mater. Sol. Cells **130**, 291–302 (2014)
20. Abderrezek, M., Djeghlal, M.E.: Comparative study on Cu2ZnSn (S, Se) 4 based thin film solar cell performances by adding various back surface field (BSF) layers. Chin. J. Phys. **63**, 231–239 (2020)
21. Ahmad, F., et al.: Towards highly efficient thin-film solar cells with a graded-bandgap CZTSSe layer. J. Phys. Energy **2**(2), 025004 (2020)
22. Et-taya, L., Ouslimane, T., Benami, A.: Numerical analysis of earth-abundant Cu2ZnSn (SxSe1-x) 4 solar cells based on Spectroscopic Ellipsometry results by using SCAPS-1D. Sol. Energy **201**, 827–835 (2020)
23. Amin, N., Sopian, K., Konagai, M.: Numerical modeling of CdS/CdTe and CdS/CdTe/ZnTe solar cells as a function of CdTe thickness. Sol. Energy Mater. Sol. Cells **91**(13), 1202–1208 (2007)
24. Plotnikov, V., et al.: Thin-film CdTe cells: reducing the CdTe. Thin Solid Films **519**(21), 7134–7137 (2011)
25. Paudel, N., Wieland, K., Compaan, A.: Ultrathin CdS/CdTe solar cells by sputtering. Sol. Energy Mater. Sol. Cells **105**, 109–112 (2012)
26. Enriquez, J.P., et al.: Influence of the film thickness on structural and optical properties of CdTe thin films electrodeposited on stainless steel substrates. Mater. Chem. Phys. **142**(1), 432–437 (2013)
27. Luo, L., et al.: High efficient and stable solid solar cell: based on FeS2 nanocrystals and P3HT: PCBM. Energy Proc. **75**, 2181–2186 (2015)
28. Xue, D.J., et al.: CuSbSe2 as a potential photovoltaic absorber material: studies from theory to experiment. Adv. Energy Mater. **5**(23), 1501203 (2015)
29. Baranowski, L.L., et al.: Effects of disorder on carrier transport in Cu 2 SnS 3. Phys. Rev. Appl. **4**(4), 044017 (2015)
30. Hossain, E.S., et al.: Performance assessment of Cu2SnS3 (CTS) based thin film solar cells by AMPS-1D. Curr. Appl. Phys. **18**(1), 79–89 (2018)
31. Razykov, T., et al.: Characterisation of SnSe thin films fabricated by chemical molecular beam deposition for use in thin film solar cells. Sol. Energy **159**, 834–840 (2018)
32. Lu, W., et al.: Melt-and air-processed selenium thin-film solar cells. Sci. China Chem. **65**(11), 2197–2204 (2022)
33. Zhou, Y., et al.: Thin-film Sb 2 Se 3 photovoltaics with oriented one-dimensional ribbons and benign grain boundaries. Nat. Photon. **9**(6), 409–415 (2015)
34. Chen, C., et al.: Optical properties of amorphous and polycrystalline Sb2Se3 thin films prepared by thermal evaporation. Appl. Phys. Lett. **107**(4), 043905 (2015)
35. Zeng, K., Xue, D.-J., Tang, J.: Antimony selenide thin-film solar cells. Semicond. Sci. Technol. **31**(6), 063001 (2016)
36. Li, Z., et al.: Sb2Se3 thin film solar cells in substrate configuration and the back contact selenization. Sol. Energy Mater. Sol. Cells **161**, 190–196 (2017)
37. Li, Z., et al.: 9.2%-efficient core-shell structured antimony selenide nanorod array solar cells. Nature Commun. **10**(1), 1–9 (2019)
38. Zhou, Y., et al.: Solution-processed antimony selenide heterojunction solar cells. Adv. Energy Mater. **4**(8), 1301846 (2014)
39. Chen, C., et al., *Characterization of basic physical properties of Sb2Se3 and its relevance for photovoltaics*. Frontiers of Optoelectronics, 2017. **10**(NREL/JA-5K00–68320).
40. Wang, L., et al.: Stable 6%-efficient Sb 2 Se 3 solar cells with a ZnO buffer layer. Nat. Energy **2**(4), 1–9 (2017)
41. Chen, S., et al.: Magnetron sputtered Sb2Se3-based thin films towards high performance quasi-homojunction thin film solar cells. Sol. Energy Mater. Sol. Cells **203**, 110154 (2019)
42. Lin, L.-Y., et al.: Analysis of Sb2Se3/CdS based photovoltaic cell: A numerical simulation approach. J. Phys. Chem. Solids **122**, 19–24 (2018)
43. Baig, F., et al.: A baseline for the numerical study of sb2se3 absorber material based solar cell. J. Nanoelectron. Optoelectron. **14**(1), 72–79 (2019)
44. Cao, Y., et al.: Towards high efficiency inverted Sb2Se3 thin film solar cells. Sol. Energy Mater. Sol. Cells **200**, 109945 (2019)
45. Baig, F., et al.: Numerical analysis of a novel CNT/Cu2O/Sb2Se3/In2S3/ITO antimony selenide solar cell. Optik **197**, 163107 (2019)
46. Li, Z.-Q., Ni, M., Feng, X.-D.: Simulation of the Sb2Se3 solar cell with a hole transport layer. Mater. Res. Exp. **7**(1), 016416 (2020)
47. Gharibshahian, I., Orouji, A.A., Sharbati, S.: Towards high efficiency Cd-Free Sb2Se3 solar cells by the band alignment optimization. Sol. Energy Mater. Sol. Cells **212**, 110581 (2020)
48. Choi, Y.C., et al.: Sb2Se3-sensitized inorganic–organic heterojunction solar cells fabricated using a single-source precursor. Angew. Chem. **126**(5), 1353–1357 (2014)
49. Liu, X., et al.: Thermal evaporation and characterization of Sb2Se3 thin film for substrate Sb2Se3/CdS solar cells. ACS Appl. Mater. Interfaces **6**(13), 10687–10695 (2014)
50. Ngo, T.T., et al.: Electrodeposition of antimony selenide thin films and application in semiconductor sensitized solar cells. ACS Appl. Mater. Interfaces **6**(4), 2836–2841 (2014)
51. Luo, M., et al.: Thermal evaporation and characterization of superstrate CdS/Sb2Se3 solar cells. Appl. Phys. Lett. **104**(17), 173904 (2014)
52. Leng, M., et al.: Selenization of Sb2Se3 absorber layer: an efficient step to improve device performance of CdS/Sb2Se3 solar cells. Appl. Phys. Lett. **105**(8), 083905 (2014)
53. Chen, C., et al.: 6.5% certified efficiency Sb2Se3 solar cells using PbS colloidal quantum dot film as hole-transporting layer. ACS Energy Lett. **2**(9), 2125–2132 (2017)
54. Wen, X., et al.: Vapor transport deposition of antimony selenide thin film solar cells with 7.6% efficiency. Nature Commun. **9**(1), 1–10 (2018)
55. Shi, J., et al.: Enhanced interface properties of solution-processed antimony sulfide planar solar cells with n-type indium sulfide buffer layer. Electrochim. Acta **376**, 138031 (2021)
56. Liu, S.-C., et al.: Boosting the efficiency of GeSe solar cells by low-temperature treatment of pn junction. Sci. China-Mater. **64**(9), 2118–2126 (2021)
57. Durose, K.: High efficiency for As-doped cells. Nat. Energy **4**(10), 825–826 (2019)
58. La Via, F., et al.: From thin film to bulk 3C-SiC growth: Understanding the mechanism of defects reduction. Mater. Sci. Semicond. Process. **78**, 57–68 (2018)
59. Metzger, W.K., et al.: Exceeding 20% efficiency with in situ group V doping in polycrystalline CdTe solar cells. Nat. Energy **4**(10), 837–845 (2019)
60. Nelson, W., Halden, F., Rosengreen, A.: Growth and Properties of β-SiC Single Crystals. J. Appl. Phys. **37**(1), 333–336 (1966)
61. Syväjärvi, M., et al.: Cubic silicon carbide as a potential photovoltaic material. Sol. Energy Mater. Sol. Cells **145**, 104–108 (2016)

62. Sobayel, M., et al.: Efficiency enhancement of CIGS solar cell by cubic silicon carbide as prospective buffer layer. Sol. Energy **224**, 271–278 (2021)
63. Burgelman, M., et al., *SCAPS Manual (version: 3.3. 07). Department of Electronics and Information Systems, University of Gent, Belgium*. 2018.
64. Basak, A., Singh, U.P.: Numerical modelling and analysis of earth abundant Sb2S3 and Sb2Se3 based solar cells using SCAPS-1D. Sol. Energy Mater. Sol. Cells **230**, 111184 (2021)
65. Sameera, J.N., et al.: Cubic Silicon Carbide (3C–SiC) as a buffer layer for high efficiency and highly stable CdTe solar cell. Opt. Mater. **123**, 111911 (2022)
66. Rahman, S., Al-Ahmed, S.R.: Photovoltaic performance enhancement in CdTe thin-film heterojunction solar cell with Sb2S3 as hole transport layer. Sol. Energy **230**, 605–617 (2021)
67. Tinedert, I., et al.: Design and simulation of a high efficiency CdS/CdTe solar cell. Optik **208**, 164112 (2020)
68. Kuddus, A., et al.: Enhancement of the performance of CdS/CdTe heterojunction solar cell using TiO2/ZnO bi-layer ARC and V2O5 BSF layers: a simulation approach. Eur. Phys. J. Appl. Phys. **92**(2), 20901 (2020)
69. Sawicka-Chudy, P., et al.: Simulation of TiO2/CuO solar cells with SCAPS-1D software. Mater. Res. Exp. **6**(8), 085918 (2019)
70. Moradi, M., et al.: Buffer layer replacement: a method for increasing the conversion efficiency of CIGS thin film solar cells. Optik **136**, 222–227 (2017)
71. Chelvanathan, P., Hossain, M.I., Amin, N.: Performance analysis of copper–indium–gallium–diselenide (CIGS) solar cells with various buffer layers by SCAPS. Curr. Appl. Phys. **10**(3), S387–S391 (2010)
72. Yaşar, S., et al.: Numerical thickness optimization study of CIGS based solar cells with wxAMPS. Optik **127**(20), 8827–8835 (2016)
73. Kanevce, A., et al.: The roles of carrier concentration and interface, bulk, and grain-boundary recombination for 25% efficient CdTe solar cells. J. Appl. Phys. **121**(21), 214506 (2017)
74. Kolsi, S., et al. *Effect of Gaussian doping profile on the performance of a thin film polycrystalline solar cell*. in *EPJ Web of Conferences*. 2012. EDP Sciences.
75. Maurya, K., Singh, V.: Sb2Se3 versus Sb2S3 solar cell: A numerical simulation. Sol. Energy **228**, 540–549 (2021)
76. Al-Ahmed, S.R., Sunny, A., Rahman, S.: Performance enhancement of Sb2Se3 solar cell using a back surface field layer: a numerical simulation approach. Solar Energy Mater. Solar Cells **221**, 110919 (2021)
77. Ali, Z., et al.: Towards the enhanced efficiency of ultrathin Sb2Se3 based solar cell with cubic silicon carbide (3C–SiC) buffer layer. Opt. Mater. **128**, 112358 (2022)
78. Ali, K., Ali, Z.: Analytical study of electrical performance of SiGe-based n+-p-p+ solar cells with BaSi2 BSF structure. Sol. Energy **225**, 91–96 (2021)
79. Kuddus, A., Ismail, A.B.M., Hossain, J.: Design of a highly efficient CdTe-based dual-heterojunction solar cell with 44% predicted efficiency. Sol. Energy **221**, 488–501 (2021)
80. Islam, A., et al.: Performance analysis of tungsten disulfide (WS2) as an alternative buffer layer for CdTe solar cell through numerical modeling. Opt. Mater. **120**, 111296 (2021)
81. Green, M.A.: General temperature dependence of solar cell performance and implications for device modelling. Prog. Photovoltaics Res. Appl. **11**(5), 333–340 (2003)
82. Theelen, M., et al.: Determination of the temperature dependency of the electrical parameters of CIGS solar cells. J. Renew. Sustain. Energy **9**(2), 021205 (2017)
83. Heriche, H., Rouabah, Z., Bouarissa, N.: New ultra thin CIGS structure solar cells using SCAPS simulation program. Int. J. Hydrogen Energy **42**(15), 9524–9532 (2017)
84. Jhuma, F.A., Shaily, M.Z., Rashid, M.J.: Towards high-efficiency CZTS solar cell through buffer layer optimization. Mater. Renew. Sustain. Energy **8**(1), 1–7 (2019)
85. Hao, X., et al. *Large Voc improvement and 9.2% efficient pure sulfide Cu 2 ZnSnS 4 solar cells by heterojunction interface engineering*. in *2016 IEEE 43rd Photovoltaic Specialists Conference (PVSC)*. 2016. IEEE.
86. Choi, Y.C., et al.: Highly improved Sb2S3 sensitized-inorganic–organic heterojunction solar cells and quantification of traps by deep-level transient spectroscopy. Adv. Funct. Mater. **24**(23), 3587–3592 (2014)